ACS OMEGA

http://pubs.acs.org/journal/acsodf

Article

Cr−Fe−Ni−Cu Quaternary Nanostructure as a Substitute for Precious Metals in Automotive Three-Way Catalysts

Taiki Hirakawa, Yuma Miyahara, Yushi Shimokawa, Koshi Nishiyama, Masayuki Tsushida, Hiroshi Yoshida, Junya Ohyama, and Masato Machida*

Cite This: *ACS Omega* 2022, 7, 44869−44877

Read Online

ACCESS | Metrics & More | Article Recommendations | Supporting Information

ABSTRACT: The replacement of precious metals (Rh, Pd, and Pt) in three-way catalysts with inexpensive and earth-abundant metal alternatives is an ongoing challenge. In this research, we examined various quaternary metal catalysts by selecting from six 3d transition metals, i.e., Cr, Mn, Fe, Co, Ni, and Cu, equimolar amounts (0.1 mol each), which were prepared on the Al_2O_3 support (1 mol Al) using H_2 reduction treatment at 900 °C. Among 15 combinations, the best catalytic performance was achieved by the CrFeNiCu system. Light-off of NO−CO−C_3H_6−O_2−H_2O mixtures proceeded at the lowest temperature of ≤200 °C for CO, ≤300 °C for C_3H_6, and ≤400 °C for NO when the molar fraction of Cr in $Cr_xFe_{0.1}Ni_{0.1}Cu_{0.1}$ was around $x = 0.1$. The activity for CO/C_3H_6 oxidation was superior to that of reference Pt/Al_2O_3 catalysts but was less active for NO reduction. The structural analysis using scanning transmission electron microscopy and X-ray absorption spectroscopy showed that the as-prepared catalyst consisted of FeNiCu alloy nanoparticles dispersed on the Cr_2O_3−Al_2O_3 support. However, the structural change occurred under a catalytic reaction atmosphere, i.e., producing NiCu alloy nanoparticles dispersed on a $NiFe_2O_4$ moiety and Cr_2O_3−Al_2O_3 support. The oxidation of CO/C_3H_6 can be significantly enhanced in the presence of Cr oxide, resulting in a faster decrease in O_2 concentration and thus regenerating the NiCu metallic surface, which is active for NO reduction to N_2.

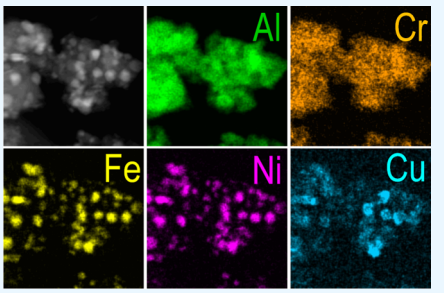

1. INTRODUCTION

Currently, the replacement of precious metals (Rh, Pd, and Pt) in three-way catalysts (TWC) with inexpensive and earth-abundant metal alternatives is a challenging topic in automotive technology, not only for conventional internal combustion engines but also for state-of-the-art hybrid-electrified powertrains. Particularly, Rh is one of the most scarce metals, with TWC accounting for more than 80% of total demand because this metal plays a crucial role in the catalytic NO reduction to N_2. Several attempts have been made in the past to replace this critical metal with other metals,[1−19] but none have been successful for widespread practical use. The high activity is closely associated with dissociative chemisorption of NO as $N_s + O_s$ (subscript s is the adsorbed species) on the Rh metal surface.[20,21] Theoretical investigations suggested that 3d transition metals (M) including Fe, Co, and Ni also facilitate the cleavage of the N−O bond and the formation of M−N_s and M−O_s bonds.[22,23] However, the as-formed M−N_s and M−O_s bonds are strong enough to monopolize the surface and hinder catalytic cycles.

Cu is a promising candidate to replace precious metals in TWC applications among 3d transition metal elements. Although several Cu-based oxide catalysts have been extensively studied from both experimental and theoretical points of view,[4,6−9,11,17,24−32] Cu metal catalysts that can easily appear under stoichiometric TWC conditions are also promising. The Cu metal surface favors nondissociative NO adsorption, but it also catalyzes NO reduction by dimerizing two NO molecules to form ONNO, followed by the N−O bond cleavage to form N_2.[33,34] The Cu metal surface's activity can further be modified by a combination with other transition metals. A NiCu alloy is one such case showing superior catalytic performance for NO reduction, as revealed by several research groups.[14,15,35−38] Tanaka et al.[35] and Asakura et al.[14,15,36] reported the higher catalytic activity of NiCu compared to its monometal counterparts. Papanikolaou and Stamatakis[39] successfully demonstrated the NiCu surface's catalytic activity in the NO−CO reactions using density functional theory combined with microkinetic modeling. We investigated various ternary 3*d* transition metal nanoparticles supported on Al_2O_3 as NO reduction catalysts in a stoichiometric NO−CO−C_3H_6−O_2−H_2O reaction.[37,38] In the presence of high-concentration H_2O, a ternary FeNiCu catalyst was discovered to have higher TWC activity and stability than unary and binary Cu-based metal nanoparticles,

Received: August 7, 2022
Accepted: November 22, 2022
Published: December 1, 2022

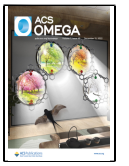

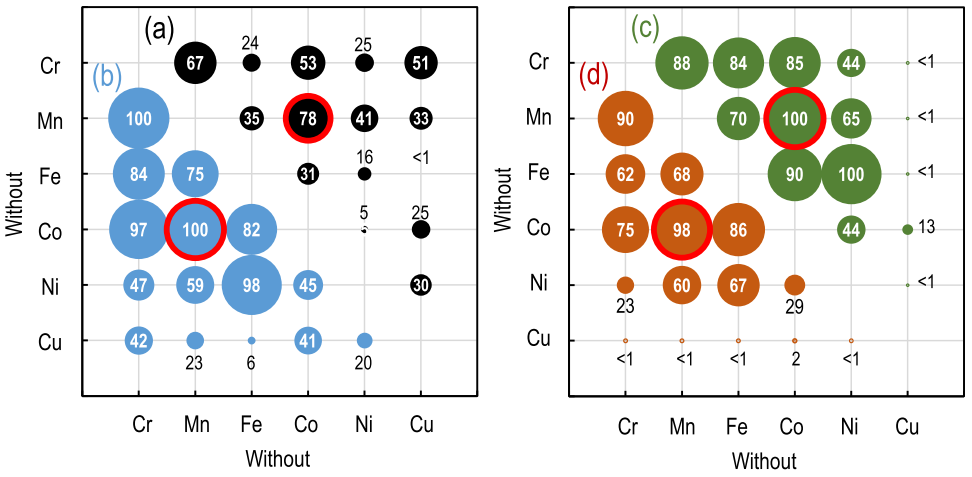

Figure 1. Conversion of NO in a stoichiometric NO−CO−C_3H_6−O_2−H_2O reaction over equimolar quaternary 3d transition metal catalysts. The composition is expressed by two elements excluded from the six elements (Cr, Mn, Fe, Co, Ni, Cu). Instantaneous NO conversion at (a) 500 °C and (b) 600 °C in the first light-off run. Steady-state NO conversion when the reaction temperature was kept at 600 °C for 1 h in (c) the first and (d) the second light-off runs. The size of the circles and numbers represents NO conversion values (%). The CrFeNiCu catalyst showing the highest activity and stability is highlighted in red.

which is associated with the regenerability of metallic species under the reaction atmosphere. The FeNiCu catalyst as prepared by H_2 reduction treatment at 900 °C consisted of single alloy nanoparticles, whereas the surface was oxidized under a low-temperature TWC atmosphere (≤300 °C). Cu and Ni reconstructed the metallic alloy nanoparticles at >300 °C, but most Fe remained fully oxidized and formed a spinel-like Fe−Ni oxide. This oxide plays a crucial role in promoting the oxidative adsorption of C_3H_6 as a carboxylate and the subsequent reaction with NO to form N_2. As oxidative C_3H_6 adsorption consumes O_2, this offers a more reductive surface environment, thus improving the stability of the active metallic state of Ni and Cu. These previous results show that the multinary 3d transition metal catalysts can offer useful and promising approaches for developing novel TWC free of Rh, Pd, and Pt. However, multinary 3d transition metal systems with more than three are not investigated systematically so far.

In this study, we examined several Al_2O_3-supported quaternary 3d transition metal systems by selecting four elements from Cr, Mn, Fe, Co, Ni, and Cu, which were prepared by a polymerized complex process followed by high-temperature H_2 reduction at 900 °C. The CrFeNiCu catalyst was found to show the highest light-off activity for a stoichiometric NO−CO−C_3H_6−O_2−H_2O gas mixture among the 15 variations of equimolar quaternary systems. Therefore, further studies were focused on Cr_xFeNiCu with different numbers of Cr molar fractions ($0 \le x \le 0.15$) to optimize the metallic composition. To reveal the role of Cr in the ternary catalysts, X-ray diffraction (XRD), X-ray absorption fine structure (XAFS) analysis, and high-angle annular dark-field scanning transmission electron microscopy (HAADF-STEM) with energy-dispersive X-ray spectrometry were applied to characterize the nanostructure and chemical state of each metal, compared with the ternary FeNiCu catalysts in our previous studies.[37,38]

2. RESULTS AND DISCUSSION

2.1. Screening of Quaternary Catalysts. Several quaternary catalysts were prepared using equimolar four elements selected from the six 3d transition elements (Cr, Mn, Fe, Co, Ni, Cu) to examine their TWC activity. Our previous study found a possible superiority of quaternary FeCoNiCu systems to ternary, binary, and unary Cu-based catalysts,[37] and this study extends this approach to the other combinations. Figure 1 illustrates representative results of the catalytic test performed in a light-off mode; the catalyst was first heated at a rate of 10 °C min^{-1} to 600 °C, where the temperature was kept constant for 1 h, followed by a ramp down to 100 °C at the same rate. In the same manner, this sequence was repeated twice (first and second runs). Here, the catalyst composition is expressed by a combination of two elements excluded from the six elements. For example, the catalyst without Co and Mn (highlighted by red fringes in Figure 1) refers to the equimolar CrFeNiCu catalyst (x = 0.10). Figure 1a,b shows the values of the instantaneous NO conversion over quaternary catalysts when the reaction temperature reaches 500 and 600 °C. The CrFeNiCu catalyst showed the fastest light-off of NO conversion (78% at 500 °C) and reached a complete conversion at 600 °C. Similar trends of catalytic activity were confirmed when the conversion of CO and C_3H_6 was used as measures instead of NO (Figure S1). Figure 1c,d compares values of the apparent NO conversion when the temperature was kept constant at 600 °C for 1 h after the first and second light-off runs. CrFeNiCu (highlighted by red fringes in Figure 1) achieved the highest conversion near 100% for both runs. In contrast, NO conversion over CrMnCoCu (without Fe and Ni) reached 100% at 600 °C in the first run but declined to 67% after a 1 h reaction at 600 °C in the second run. We chose CrFeNiCu as the possible candidate since it had the lowest light-off temperature and highest conversion at 600 °C. This result confirmed our previous findings, demonstrating that FeNiCu was the most active among the ternary systems, and showed the positive effect of adding Cr to enhance the activity. The activity tends to be very low when Cu is not contained in the quaternary systems (Figure 1), indicating that this element is crucial and thus indispensable in substituting the function of precious metals in TWC.

In the following, further studies were focused on the TWC light-off characteristics of the quaternary Cr_xFeNiCu catalyst system with different amounts of Cr added ($0 \le x \le 0.15$).

https://doi.org/10.1021/acsomega.2c05043
ACS Omega 2022, 7, 44869−44877

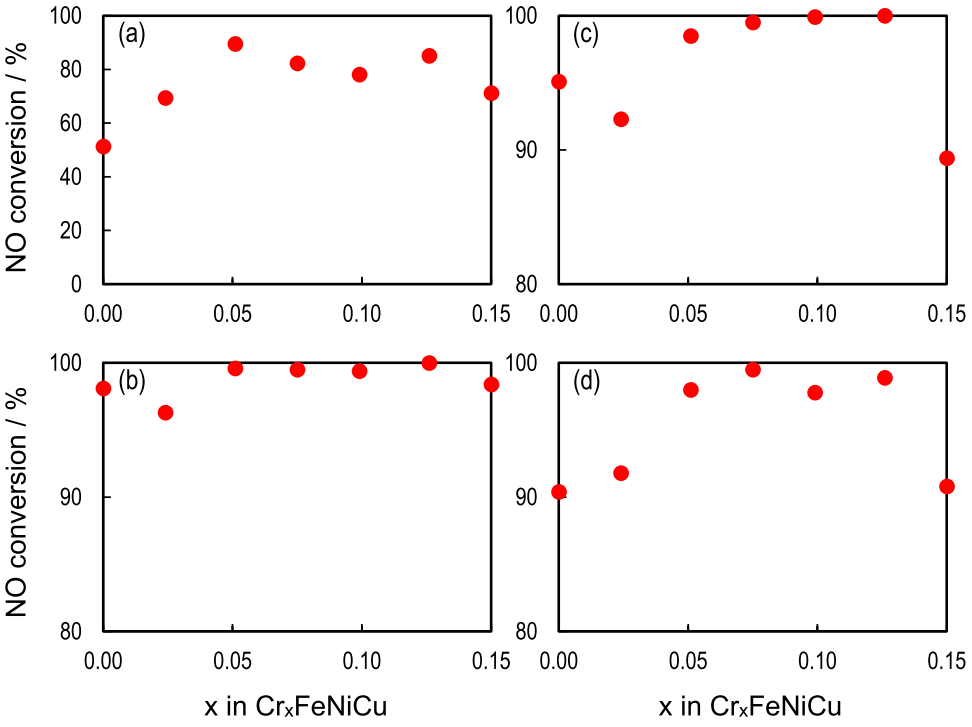

Figure 2. Conversion of NO in a stoichiometric NO−CO−C_3H_6−O_2−H_2O reaction over $Cr_xFeNiCu$ catalysts ($0 \leq x \leq 0.15$). Instantaneous NO conversion at (a) 500 °C and (b) 600 °C in the first light-off run. Steady-state NO conversion when the reaction temperature was kept at 600 °C for 1 h in (c) the first and (d) the second light-off runs.

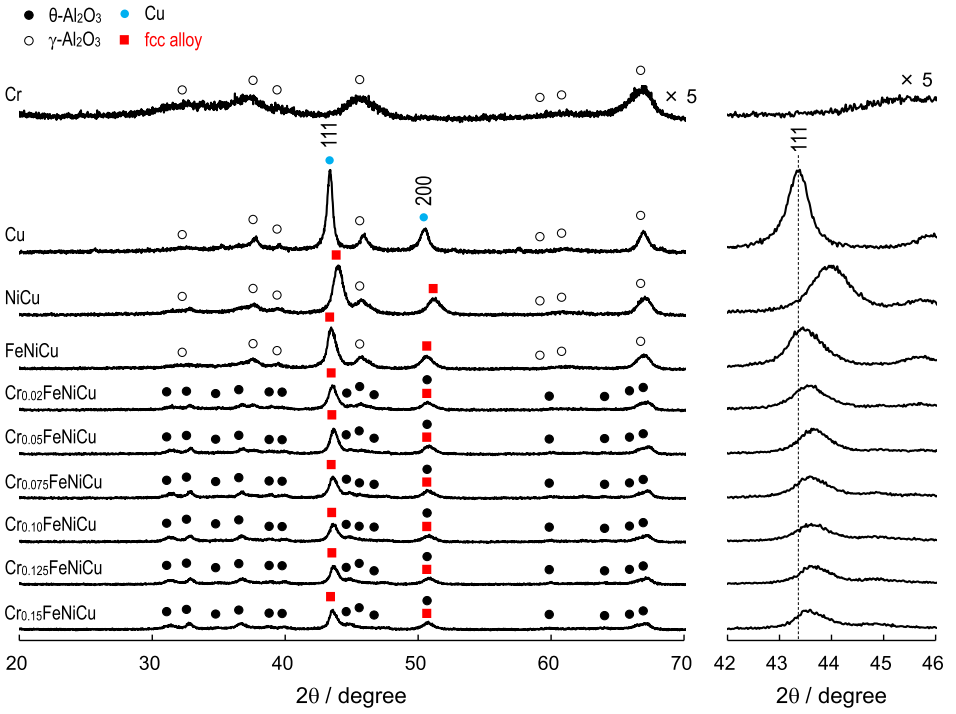

Figure 3. XRD patterns of $Cr_xFeNiCu$ catalysts after H_2 reduction at 900 °C. Enlarged parts around the main peaks are shown on the right.

The instantaneous NO conversion at 500 and 600 °C during the first light-off tended to increase with the addition of Cr, as shown in Figure 2a,b, showing the highest value at about x = 0.05−0.125 (see Figures S2 and S3 for each data). A similar trend was observed in the NO conversion after the reaction temperature was kept at 600 °C for 1 h (first run: Figure 2c and second run: Figure 2d). However, further Cr addition of more than x = 0.125 resulted in a negative effect on the catalytic activity. Despite the Cr amount, the S_{BET} was similar around 32−36 m^2 g^{-1} (Table S2). Thus, the activity improvement cannot be explained by a simple surface area effect. The product selectivity to N_2 at these temperatures was more than 95%. We decided on the optimum composition at x = 0.10, which was primarily applied in the following

https://doi.org/10.1021/acsomega.2c05043
ACS Omega 2022, 7, 44869−44877

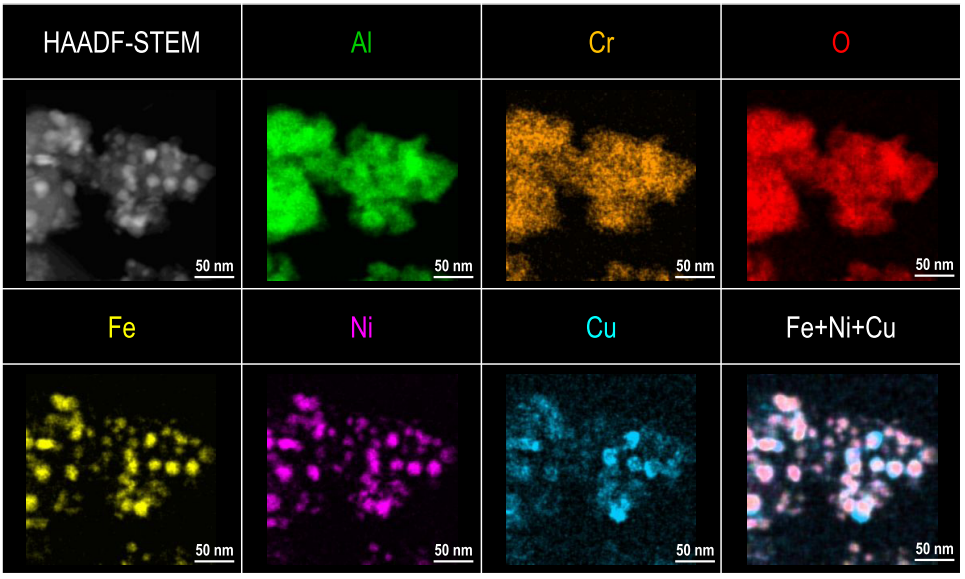

Figure 4. HAADF-STEM and X-ray mapping images of the $Cr_{0.10}FeNiCu$ catalyst after H_2 reduction at 900 °C for 3 h.

characterization investigations. Since the optimal addition of Cr was found to considerably improve the catalytic activity, our interest is to elucidate the possible mechanism of how Cr modifies the structure and catalytic function. The $Cr_{0.10}FeNiCu$ catalyst was superior for the CO/C_3H_6 oxidation activity but inferior for the NO reduction activity when compared with those of Rh and Pt catalysts (Figure S4).

2.2. Structure of $Cr_xFeNiCu$ After H_2 Reduction and Subsequent Catalytic Reaction. Figure 3 illustrates the XRD patterns of $Cr_xFeNiCu$ and reference catalysts after H_2 reduction at 900 °C. The Cu-only catalyst shows two sharp peaks of the 111 and 200 reflections of the face-centered cubic (fcc) Cu metal ($Fm\bar{3}m$, a = 3.614 Å). However, the Cr-only catalyst shows no metallic phase but weak reflections due to γ-Al_2O_3. The binary NiCu catalyst showed peaks of the fcc metal, but their positions were shifted to higher 2θ, indicating the formation of NiCu alloys with a smaller lattice constant (a = 3.564 Å).[40] In the ternary FeNiCu, a single fcc alloy phase was also formed, with the peak positioned between the Cu and NiCu cases. This is consistent with the reported lattice constant of $Fe_{0.21}Ni_{0.50}Cu_{0.29}$ (a = 3.579 Å), which is larger than that of NiCu and smaller than that of Cu.[41] Judging from the XRD and STEM experiments in our previous studies,[37,38] NiCu and FeNiCu are considered as random alloys, whereas their surface structures are unclear because of partial oxidation to different extents. Notably, almost the same diffraction peak positions were preserved in the quaternary systems ($Cr_xFeNiCu$, $0 < x \leq 0.15$), regardless of the amount of Cr. A slight deviation of the 111 peak position and decreased intensity was observed, but this was probably due to the inhomogeneous composition of the FeNiCu alloy nanoparticles. Another point to be noted is the appearance of broad and weak peaks of θ-Al_2O_3, which were not observed for unary, binary, and ternary Cu catalysts. Additionally, XANES analysis of H_2-treated $Cr_xFeNiCu$ samples showed that Fe, Ni, and Cu were in a metallic state, whereas Cr was almost oxidized (Cr^{3+}) (Figure S5). Similarly, the XPS analysis of the catalyst surface suggested the presence of metallic species (Fe^0, Ni^0, and Cu^0), but Cr was only in the state of Cr^{3+} (Figure S6).

HAADF-STEM and X-ray element mapping were used to examine the nanoscale distribution of each metal element in the H_2-reduced quaternary catalysts ($Cr_{0.10}FeNiCu$). As shown in Figure 4, Fe, Ni, and Cu showed a roughly similar distribution and thus coincided with the formation of the ternary FeNiCu alloy particles of about 10−20 nm in size. However, the stronger Cu element signal near the outer periphery of each particle suggested that Cu may be enriched near the surface of alloy nanoparticles. Unlike these elements, Cr, Al, and O distributions spread over several hundred nanometers and well-overlapped each other. These findings indicate the formation of the ternary FeNiCu alloy nanoparticles deposited on the binary oxide support of Cr_2O_3−Al_2O_3. This was consistent with the results of XRD (Figure 3), XANES (Figure S5), and XPS (Figure S6). Thus, the Cr species in the quaternary compounds exist as an oxide phase but not as a metallic phase. There is a series of solid solutions in the phase diagram of Cr_2O_3 and Al_2O_3.[42,43] According to Ozawa et al.,[44] Cr^{3+} can be dissolved in θ-Al_2O_3 to form a pseudo solid solution at 800−1000 °C. This could explain why the θ-Al_2O_3 phase was dominant in $Cr_xFeNiCu$, whereas Cu, NiCu, and FeNiCu contained γ-Al_2O_3.

The oxidation state and the nanostructure of quaternary $Cr_xFeNiCu$ catalysts changed substantially under stoichiometric NO−CO−C_3H_6−O_2−H_2O reaction conditions. Figure 5 compares the obvious conversion of NO, CO, and C_3H_6 over FeNiCu and $Cr_{0.10}FeNiCu$ catalysts during temperature ramping to 600 °C (10 °C min^{-1}), followed by holding at this temperature for 1 h. The Cr addition improved the light-off performance and enhanced the stability at 600 °C. Furthermore, Figure 5 shows the plots of the fraction of metallic states of each element (Cu^0, Ni^0, and Fe^0), which was determined using XANES (see Figure S7 for each data). Fe, Ni, and Cu in the H_2-reduced catalysts were present in their respective metallic states (Cu^0/Cu = Ni^0/Ni = Fe^0/Fe = 100%), as described above, whereas the metallic fraction dropped steeply at the beginning of catalytic reactions at <300 °C due to the oxidation by unreacted O_2. In the case of FeNiCu, Cu^0/Cu demonstrated the greatest drop to <40% but immediately recovered the initial value with the progress of

https://doi.org/10.1021/acsomega.2c05043
ACS Omega 2022, 7, 44869−44877

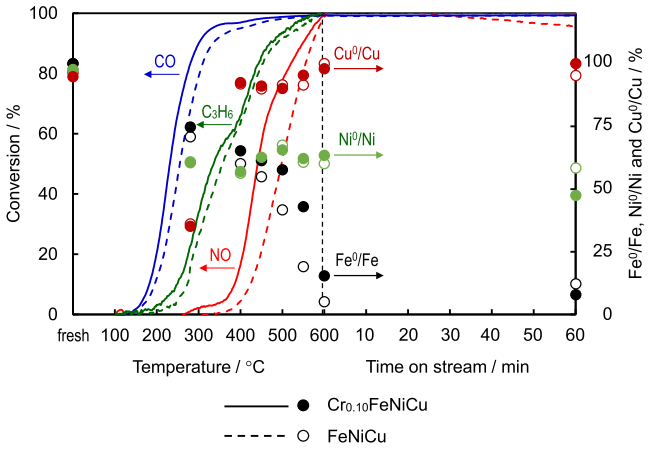

Figure 5. Relationship between the catalytic NO, CO, and C_3H_6 conversion and the fraction of metallic state for the $Cr_xFeNiCu$ catalyst (x = 0 and 0.10) during the stoichiometric NO−CO−C_3H_6−O_2−H_2O reaction in a light-off mode (10 °C min^{-1}), followed by an isothermal mode (600 °C for 1 h).

temperature increase higher than 300 °C, where the O_2 partial pressure decreased by the oxidation of CO/C_3H_6. Furthermore, Ni^0/Ni fraction decreased monotonically but kept at around 50% during the isothermal reaction at 600 °C for 1 h. However, Fe^0/Fe decreased with an increasing rate to less than 10%, indicating the lowest stability against oxidation. A similar change was observed for $Cr_{0.10}$FeNiCu, but the Fe oxidation during the light-off was retarded slightly in the presence of Cr.

Figure 6 shows the X-ray mapping images of $Cr_{0.10}$FeNiCu after treatment at 600 °C for 1 h under a flow of a stoichiometric NO−CO−C_3H_6−O_2−H_2O gas mixture. In contrast to the H_2-reduced sample (Figure 4), where the distribution of Fe, Ni, and Cu was nearly identical, these three elements showed different distributions after exposure to the catalytic reaction atmosphere. Although Cu was still confined to an area of 10−20 nm in size as in the fresh catalyst (Figure 4), the distributions of Fe and Ni spread over the Cr_2O_3−Al_2O_3 support because of oxidation. The nearly identical distribution between Fe and Ni indicates the formation of mixed oxides, such as $NiFe_2O_4$. Considering the 1:2 ratio of $NiFe_2O_4$, the remaining Ni may be in the form of CuNi alloy, as shown in Figure 5. Previously, we reported a similar structural change that occurred in the ternary FeNiCu catalyst when exposed to the reaction gas mixture.[38] Based on these characterization results, the local structural change under the catalytic reaction condition is schematically inferred, as illustrated in Scheme 1. In the fresh catalyst after H_2 reduction

Scheme 1. Structural Change of the CrFeNiCu Catalyst Under a Stoichiometric NO−CO−C_3H_6−O_2−H_2O Reaction

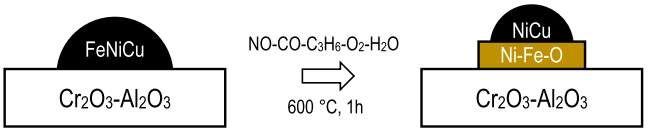

at 900 °C, the FeNiCu alloy particles were deposited on the Cr_2O_3−Al_2O_3 support. Under the TWC conditions at 600 °C, the alloy nanoparticle was oxidized to some extent and transformed into a structure consisting of NiCu alloy nanoparticles and $NiFe_2O_4$ oxides, which were dispersed on the Cr_2O_3−Al_2O_3 support.

2.3. Effect of Cr on the TWC Activity of Cr_xFeNiCu.

Since the FeNiCu alloy nanoparticles in the H_2-reduced FeNiCu and $Cr_{0.10}$FeNiCu transformed into NiCu alloy nanoparticles and $NiFe_2O_4$ moieties under the reaction atmosphere (Scheme 1), the effect of Cr on the catalytic activity was investigated in further detail using 12 model reactions (CO−NO, CO−O_2, C_3H_6−O_2, and so on, see Table S1 for detail). For this purpose, the catalysts were pretreated at 600 °C for 1 h under a flow of a stoichiometric NO−CO−C_3H_6−O_2−H_2O gas mixture. Figure 7 illustrates the radar chart that plots the value of T_{50}, which is the temperature at which the conversion of the underlined gas species (NO, CO, or C_3H_6) reached 50% (see Figure S8 for each reaction data). Therefore, a lower T_{50} indicates a higher catalytic activity. The

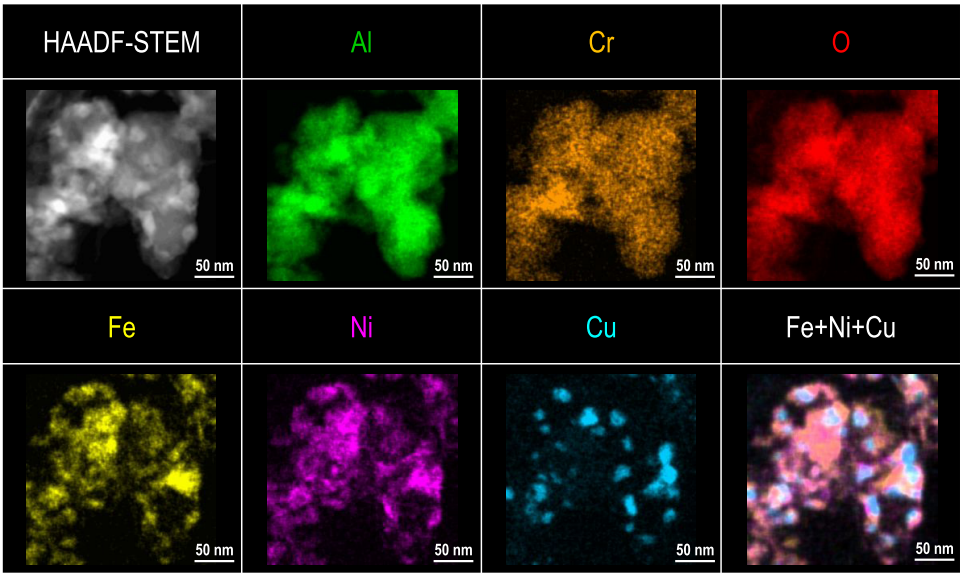

Figure 6. HAADF-STEM and X-ray mapping images of the $Cr_{0.10}$FeNiCu catalyst after the treatment in a stoichiometric NO−CO−C_3H_6−O_2−H_2O reaction at 600 °C for 1 h.

https://doi.org/10.1021/acsomega.2c05043
ACS Omega 2022, 7, 44869−44877

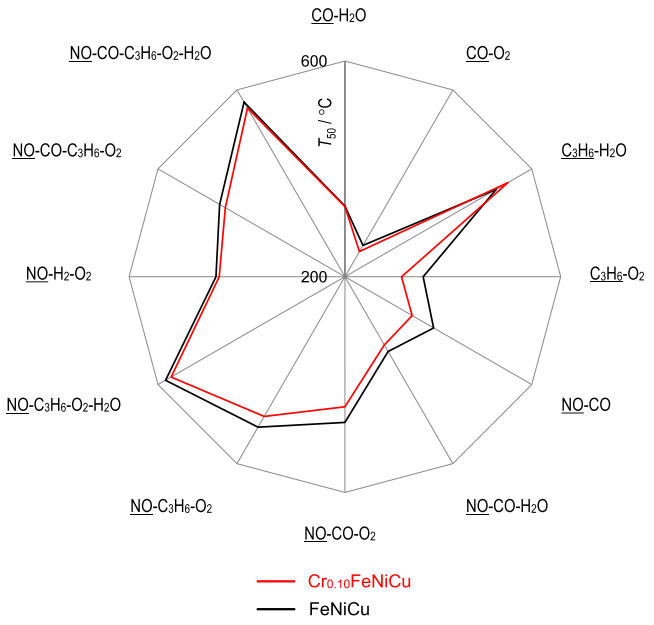

Figure 7. Catalytic activities of $Cr_{0.10}FeNiCu$ and FeNiCu catalysts for various TWC-related reactions. The T_{50} values for the underlined gases are plotted. The catalysts were pretreated during a stoichiometric NO−CO−C_3H_6−O_2−H_2O reaction at 600 °C for 1 h.

activity distributions of these catalysts were similar; however, $Cr_{0.10}FeNiCu$ was more active than FeNiCu in almost all cases except a C_3H_6−H_2O reaction. Notably, significant superiority of $Cr_{0.10}FeNiCu$ was observed for C_3H_6−O_2 and NO−C_3H_6−O_2 reactions. As we previously reported,[38] the copresence of NiCu alloys and $NiFe_2O_4$ enhances the oxidative adsorption of C_3H_6 to form a carboxylate, which plays a crucial role as a reducing agent for NO reduction to N_2 over the NiCu nanoparticles. Following the same approach, we examined the formation and reaction of surface adsorption species on the present $Cr_{0.10}FeNiCu$ catalyst applying in situ FTIR combined with an isotopic pulse reaction approach (Figures S9 and S10). Since the formation of carboxylate was further enhanced on $Cr_{0.10}FeNiCu$ compared to FeNiCu, the role of Cr is considered to promote the oxidative adsorption of C_3H_6, which provides a more reductive surface environment, thereby increasing the stability of the active metallic state. Considering lower light-off temperatures for CO (≥150 °C) and C_3H_6 (≥200 °C) for $Cr_{0.10}FeNiCu$ in Figure 5, the resulting lower O_2 concentration should be suitable for not only mitigating the oxidation of the metallic surface but also regenerating the metallic surface. Part of the added Cr may be incorporated into the $NiFe_2O_4$ moiety to form a multinary oxide phase. According to our previous study,[12,45] the incorporation of Cr into spinel oxides such as in $Cu_{0.05}Ni_{0.95}Al_yCr_{2-y}O_4$ effectively improves the activity for C_3H_6−O_2 reactions.

When the metallic state of Cu-based alloys can be reconstructed in the presence of Cr, a positive effect on the NO reduction efficiency is expected. The 3*d* transition metals facilitate dissociative and/or nondissociative adsorption of NO molecules,[20,21] depending on the *d*-valence orbital energy,[22,23,33,34,46−48] which increases in the order of Fe > Co > Ni ≫ Cu. According to this order, the N−O bond cleavage and the resulting formation of M−N_s and M−O_s bonds are expected to be more favorable on Fe and Ni rather than Cu. However, the stronger the M−N_s and M−O_s bonds, the more difficult the removal of N_s and O_s adatoms from the metal surface. Thus, we face a trade-off between the NO dissociation rate and the N_s/O_s removal rate. Figure 8 illustrates the NO

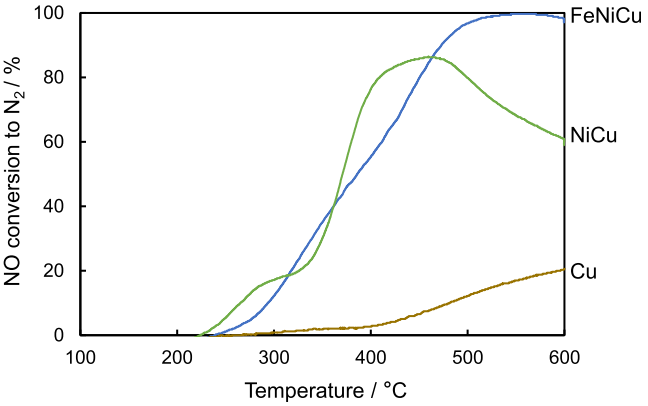

Figure 8. NO conversion to N_2 over FeNiCu, NiCu, and Cu catalysts during temperature ramping (10 °C min^{-1}) in a stream of 0.05% NO/He. The catalysts were reduced by H_2 at 900 °C for 3 h.

conversion to N_2 during the temperature ramping of the catalysts in a stream of 0.05% NO/He. Cu alone produced the least conversion of NO to N_2 since the nondissociative NO adsorption is favored, as described above. However, NiCu and FeNiCu produced considerably higher amounts of N_2 than Cu alone because Fe and Ni are more active in the dissociative NO adsorption. As the reaction product contained negligible amounts of O_2 and N_2O, the observed N_2 evolution can be considered as the following solid−gas reaction

$$NO_s + M \rightarrow \frac{1}{2}N_2 + M - O_s \quad (1)$$

where M is Fe, Ni, and/or Cu. The total amount of NO converted to N_2 was close to those estimated from reaction 1, suggesting that not only the surface but also bulk metal species were oxidized by NO. With the progress of the solid−gas reaction, the rate of the reaction will be determined by the thickness of the oxidized surface layer (M−O_s), as can be seen in the case of NiCu in Figure 8. Finally, NO conversion will suspend when the metallic species are consumed completely by reaction 1. Nevertheless, reaction 1 can be cycled when the M−O_s is reduced to the M under a NO−CO−C_3H_6−O_2−H_2O gas mixture. Thus, the higher oxidation activity for CO/C_3H_6 of $Cr_{0.10}FeNiCu$ achieves a lower O_2 concentration favorable for the regeneration from M−O_s to M and thus realizes more efficient catalytic cycles of NO reduction.

3. METHODS AND MATERIALS

3.1. Catalyst Preparation. CrFeNiCu quaternary catalysts supported on Al_2O_3 were prepared using a polymerized complex process and a post-H_2-reduction treatment, which was used in our previous study to prepare the FeNiCu ternary system.[37,38] The molar ratio of Cr/Fe/Ni/Cu/Al = *x*:0.1:0.1:0.1:1.0 ($0 \le x \le 0.15$) was expressed using a general formula, Cr_xFeNiCu. Calculated amounts (total amounts = 26 + 20*x* mmol) of $Cr(NO_3)_3$, $Fe(NO_3)_3$, $Ni(NO_3)_2$, $Cu(NO_3)_2$, and $Al(NO_3)_3$ (Wako Pure Chemical Industries, Japan) and citric acid (300 mmol) (Wako Pure Chemical Industries, Japan) were added in distilled and deionized water (180 mL) and stirred vigorously at 80 °C for 2 h. Under vigorous stirring, ethylene glycol (300 mmol) (Wako Pure Chemical Industries,

https://doi.org/10.1021/acsomega.2c05043
ACS Omega 2022, 7, 44869−44877

Japan) was added to the as-obtained clear solution. When stirred at 80 °C for 8 h, the solution was gradually changed into a viscous gel, which was heated at 130 °C for 2 h. Then, the solid product was calcined for 1 h at 600 °C and 900 °C for 2 h. To produce Al_2O_3-supported metal catalysts, the oxide precursor thus obtained was ground into powder using an agate mortar and was finally heated for 3 h at 900 °C under flowing H_2. The other quaternary metal catalysts were prepared in the same manner by selecting from six 3*d* transition metals, i.e., Cr, Mn, Fe, Co, Ni, and Cu.

3.2. Characterization. To determine the Brunauer−Emmett−Teller surface area (S_{BET}), N_2 adsorption isotherms were measured at −196 °C using a Belsorp Mini instrument (Microtrac-Bel, Japan). XRD was applied to determine the crystal structure using a Rigaku Multiflex diffractometer (Japan) with monochromatic Cu Kα radiation (30 kV, 30 mA). An X-ray fluorescence spectrometer (EDXL300, Rigaku, Japan) was used to determine the metal composition and was nearly equal to the expected values. An FEI Tecnai F20 (Thermo Scientific) instrument operating at 200 kV was used to perform HAADF-STEM and energy-dispersive X-ray analyses. A K-Alpha spectrometer (Thermo Scientific) under 12 kV Al Kα radiation was applied to obtain surface analysis via X-ray photoelectron spectroscopy (XPS). The samples were reduced by H_2 at 900 °C and/or treated under catalytic reaction conditions, as described below, before being transferred to an XPS chamber under vacuum with no air exposure. The C 1s peak (285.0 eV) was applied as an internal reference to correct the observed binding energies for surface charging.

XAFS measurement on K-edges of Cr, Fe, Ni, and Cu was performed at the BL14B2 station at SPring-8 in Japan Synchrotron Radiation Research Institute in transmission mode using a Si(111) double-crystal monochromator. In a N_2-filled ionization chamber (17 cm in length) and a 50% N_2/Ar-filled ionization chamber (31 cm in length), the intensities of the incident and transmitted X-rays were monitored, respectively. To ensure appropriate absorbance at the edge energy during the XAFS analysis, the powder sample was pressed onto a disk (diameter = 7 mm). Before the measurement, the sample was pretreated by a water-cooled infrared image furnace (Ulvac RHL-E25, Japan) under a stream of stoichiometric NO−CO−C_3H_6−O_2−H_2O gas mixture and was flushed with He, followed by quick cooling to ambient temperature. The as-treated sample was sealed in a polyethylene bag under dry Ar and transferred without exposure to air. X-ray absorption near-edge structures (XANES) were applied to determine the oxidation states of Cr, Fe, Ni, and Cu using a linear combination fitting approach. A cubic spline approach throughout the postedge regions was applied to extract the oscillatory part in *k*-space. Athena software was used to perform data processing,[49] and reference samples were obtained from the metal foils and metal oxides.

3.3. Catalytic Reactions. In a flow microreactor under atmospheric pressure, the catalytic test for simulated TWC reactions was conducted. A mixture of 0.05% NO, 0.50% CO, 0.04% C_3H_6, 0.40% O_2, and 5.0% H_2O, balanced by He, supplied the granular catalyst (W = 50 mg, 20 mesh), which was packed in a quartz tube (inside diameter = 4 mm) at a flow rate of F = 100 cm^3 min^{-1} ($W/F = 5 \times 10^{-4}$ g min cm^{-3}). This mixture corresponded to a stoichiometric air-to-fuel weight ratio, indicating that all gases could be completely converted into a mixture of CO_2, H_2O, and/or N_2 with no residual trace of O_2. An infrared image furnace heated the catalytic bed from 100 to 600 °C at a constant rate of 10 °C min^{-1}. A nondispersive infrared gas analyzer (VA-3000, Horiba, Japan) and a magneto-pneumatic O_2 analyzer (Horiba MPA3000, Japan) were used to determine NO, N_2O, CO, and C_3H_6 concentrations. Furthermore, the catalytic activity test was conducted similarly for various model reactions, including CO−O_2, C_3H_6−O_2, NO−CO, NO−C_3H_6−O_2, and NO−CO−O_2 (see Table S1).

In situ FTIR spectra of the adsorbed gas species were acquired on a Thermo Scientific Nicolet iS50 spectrometer using a temperature-controllable diffuse reflectance reaction cell as described in our previous paper.[38] For this purpose, model catalysts with a lower metal loading of (Fe + Ni + Cu)/Al = 0.03:1.0 were pretreated in the stoichiometric NO−CO−C_3H_6−O_2−H_2O mixture at 600 °C for 1 h. The sample was heated in situ under the flow of He at 500 °C for 30 min (50 cm^3 min^{-1}), followed by cooling to 400 °C, where the gas feed was changed to a mixture of 0.10% C_3H_6, 0.46% O_2, and He balance for 10 min. After He flushing, 0.78% NO/He was supplied for 10 min. Meanwhile, spectral measurements were recorded at 1 min intervals.

4. CONCLUSIONS

Quaternary 3d transition metal catalysts supported on Al_2O_3 were prepared using a polymerized complex approach and a high-temperature H_2 reduction treatment (900 °C). Among equimolar quaternary catalysts, the combination of CrFeNiCu was discovered to achieve the maximum NO reduction efficiency in a stoichiometric NO−CO−C_3H_6−O_2−H_2O reaction that simulates automotive TWC. At a molar ratio of Cr/Fe/Ni/Cu/Al = 0.05−0.125:0.1:0.1:0.1:1.0, the metal composition was optimized, where the activity for CO/C_3H_6 oxidation was superior to that of the reference Rh and Pt catalysts but was less active for NO reduction. Fe, Ni, and Cu formed alloy nanoparticles in the H_2-reduced catalysts, whereas Cr was present as Cr_2O_3−Al_2O_3 support. The FeNiCu alloy was promptly oxidized under a TWC atmosphere, and the catalyst comprised NiCu alloy nanoparticles deposited on the Fe−Ni oxide formed on Cr_2O_3−Al_2O_3. The oxidation of CO/C_3H_6 can be significantly enhanced in the presence of Cr oxide, resulting in a faster decrease in O_2 concentration that is favorable for reconstructing NiCu metallic alloys, which is active in NO reduction to N_2.

■ ASSOCIATED CONTENT

Supporting Information

The Supporting Information is available free of charge at https://pubs.acs.org/doi/10.1021/acsomega.2c05043.

Catalytic activity tests, isotope reactions, surface area, XAFS, XPS, FTIR results, and reaction conditions (PDF)

■ AUTHOR INFORMATION

Corresponding Author

Masato Machida − *Division of Materials Science and Chemistry, Faculty of Advanced Science and Technology and Institute of Industrial Nanomaterials, Kumamoto University, Kumamoto 860-8555, Japan; Elements Strategy Initiative for Catalysts and Batteries, Kyoto University, Kyoto 615-8245, Japan;* orcid.org/0000-0002-6207-7914;
Email: machida@kumamoto-u.ac.jp

https://doi.org/10.1021/acsomega.2c05043
ACS Omega 2022, 7, 44869−44877

Authors

Taiki Hirakawa − *Department of Applied Chemistry and Biochemistry, Graduate School of Science and Technology, Kumamoto University, Kumamoto 860-8555, Japan*

Yuma Miyahara − *Department of Applied Chemistry and Biochemistry, Graduate School of Science and Technology, Kumamoto University, Kumamoto 860-8555, Japan*

Yushi Shimokawa − *Department of Applied Chemistry and Biochemistry, Graduate School of Science and Technology, Kumamoto University, Kumamoto 860-8555, Japan*

Koshi Nishiyama − *Department of Applied Chemistry and Biochemistry, Graduate School of Science and Technology, Kumamoto University, Kumamoto 860-8555, Japan*

Masayuki Tsushida − *Technical Division, Kumamoto University, Kumamoto 860-8555, Japan*

Hiroshi Yoshida − *Division of Materials Science and Chemistry, Faculty of Advanced Science and Technology, Kumamoto University, Kumamoto 860-8555, Japan; Elements Strategy Initiative for Catalysts and Batteries, Kyoto University, Kyoto 615-8245, Japan;* orcid.org/0000-0001-9570-477X

Junya Ohyama − *Division of Materials Science and Chemistry, Faculty of Advanced Science and Technology and Institute of Industrial Nanomaterials, Kumamoto University, Kumamoto 860-8555, Japan; Elements Strategy Initiative for Catalysts and Batteries, Kyoto University, Kyoto 615-8245, Japan;* orcid.org/0000-0002-7438-5236

Complete contact information is available at: https://pubs.acs.org/10.1021/acsomega.2c05043

Author Contributions

T.H., Y.M., Y.S., and K.N. performed the catalyst preparation, characterization, and catalytic reactions. M.T., H.Y., and J.O. performed the characterization. M.M. proposed, planned, and designed the research. This manuscript was written with contributions from all named authors, and each author approved the final version of the manuscript.

Notes

The authors declare no competing financial interest.

■ ACKNOWLEDGMENTS

This work was supported by the Ministry of Education, Culture, Sports, Science and Technology (MEXT) program, "Element Strategy Initiative to Form Core Research Center (JPMXP0112101003)," which has been run by MEXT, Japan, since 2012, and Japan Society for the Promotion of Science (JSPS) KAKENHI Grant Number 22H00277. T.H. acknowledges the Grant-in-Aid for JSPS Research Fellow Number 21J11616. The XAFS experiments were performed at the beamline BL15 of the SAGA Light Source (Proposal No. 2107092R/BL15) and the BL14B2 beamline of SPring-8 (Proposal Nos. 2019B1909 and 2021A1657).

■ REFERENCES

(1) Libby, W. F. Promising Catalyst for Auto Exhaust. *Science* **1971**, *171*, 499−500.

(2) Tanaka, H.; Uenishi, M.; Taniguchi, M.; Tan, I.; Narita, K.; Kimura, M.; Kaneko, K.; Nishihata, Y. Mizuki, J. i., The Intelligent Catalyst Having the Self-Regenerative Function of Pd, Rh and Pt for Automotive Emissions Control. *Catal. Today* **2006**, *117*, 321−328.

(3) Royer, S.; Duprez, D.; Can, F.; Courtois, X.; Batiot-Dupeyrat, C.; Laassiri, S.; Alamdari, H. Perovskites as Substitutes of Noble Metals for Heterogeneous Catalysis: Dream or Reality. *Chem. Rev.* **2014**, *114*, 10292−10368.

(4) Glisenti, A.; Pacella, M.; Guiotto, M.; Natile, M. M.; Canu, P. Largely Cu-Doped $LaCo_{1-x}Cu_xO_3$ Perovskites for TWC: Toward New PGM-Free Catalysts. *Appl. Catal., B* **2016**, *180*, 94−105.

(5) Ueda, K.; Ang, C. A.; Ito, Y.; Ohyama, J.; Satsuma, A. $NiFe_2O_4$ as an Active Component of a Platinum Group Metal-Free Automotive Three-Way Catalyst. *Catal. Sci. Technol.* **2016**, *6*, 5797−5800.

(6) Perin, G.; Fabro, J.; Guiotto, M.; Xin, Q.; Natile, M. M.; Cool, P.; Canu, P.; Glisenti, A. $Cu@LaNiO_3$ Based Nanocomposites in TWC Applications. *Appl. Catal., B* **2017**, *209*, 214−227.

(7) Garbujo, A.; Pacella, M.; Natile, M. M.; Guiotto, M.; Fabro, J.; Canu, P.; Glisenti, A. On A-Doping Strategy for Tuning the TWC Catalytic Performance of Perovskite Based Catalysts. *Appl. Catal., A* **2017**, *544*, 94−107.

(8) Pacella, M.; Garbujo, A.; Fabro, J.; Guiotto, M.; Xin, Q.; Natile, M. M.; Canu, P.; Cool, P.; Glisenti, A. PGM-Free $CuO/LaCoO_3$ Nanocomposites: New Opportunities for TWC Application. *Appl. Catal., B* **2018**, *227*, 446−458.

(9) Schön, A.; Dacquin, J.-P.; Granger, P.; Dujardin, C. Non Stoichiometric $La_{1-y}FeO_3$ Perovskite-Based Catalysts as Alternative to Commercial Three-Way-Catalysts? − Impact of Cu and Rh Doping. *Appl. Catal., B* **2018**, *223*, 167−176.

(10) Carollo, G.; Garbujo, A.; Xin, Q.; Fabro, J.; Cool, P.; Canu, P.; Glisenti, A. $CuO/La_{0.5}Sr_{0.5}CoO_3$ Nanocomposites in TWC. *Appl. Catal., B* **2019**, *255*, No. 117753.

(11) Ueda, K.; Tsuji, M.; Ohyama, J.; Satsuma, A. Tandem Base-Metal Oxide Catalyst: Superior NO Reduction Performance to the Rh Catalyst in $NO−C_3H_6−CO−O_2$. *ACS Catal.* **2019**, *9*, 2866−2869.

(12) Hirakawa, T.; Shimokawa, Y.; Tokuzumi, W.; Sato, T.; Tsushida, M.; Yoshida, H.; Hinokuma, S.; Ohyama, J.; Machida, M. Multicomponent Spinel Oxide Solid Solutions: A Possible Alternative to Platinum Group Metal Three-Way Catalysts. *ACS Catal.* **2019**, *9*, 11763−11773.

(13) Yoshida, H.; Kawakami, Y.; Tokuzumi, W.; Shimokawa, Y.; Hirakawa, T.; Ohyama, J.; Machida, M.; Low-Temperature, N. O. Reduction over Fe−Ni Alloy Nanoparticles Using Synergistic Effects of Fe and Ni in a Catalytic $NO−CO−C_3H_6−O_2$ Reaction. *Bull. Chem. Soc. Jpn.* **2020**, *93*, 1050−1055.

(14) Asakura, H.; Onuki, T.; Hosokawa, S.; Takagi, N.; Sakaki, S.; Teramura, K.; Tanaka, T. Self-Regeneration of a Ni−Cu Alloy Catalyst During a Three-Way Catalytic Reaction. *Phys. Chem. Chem. Phys.* **2019**, *21*, 18816−18822.

(15) Asakura, H.; Kirihara, M.; Fujita, K.; Hosokawa, S.; Kikkawa, S.; Teramura, K.; Tanaka, T. Fe-Modified CuNi Alloy Catalyst as a Nonprecious Metal Catalyst for Three-Way Catalysis. *Ind. Eng. Chem. Res.* **2020**, *59*, 19907−19917.

(16) Brusamarello, E.; Blonda, C.; Salazar-Castro, C.; Pascui, A. E.; Canu, P.; Glisenti, A. Industrially Produced Fe- and Mn-Based Perovskites: Effect of Synthesis on Reactivity in Three-Way Catalysis: Part 1. *ACS Omega* **2021**, *6*, 24325−24337.

(17) Yoshida, H.; Oyama, H.; Shiomori, R.; Hirakawa, T.; Ohyama, J.; Machida, M. Enhanced Catalytic NO Reduction in $NO−CO−C_3H_6−O_2$ Reaction Using Pseudo-Spinel $(NiCu)Al_2O_4$ Supported on γ-Al_2O_3. *ACS Catal.* **2021**, *11*, 7302−7309.

(18) Nandi, S.; Wu, J. X.; Simon, P.; Nuns, N.; Trentesaux, M.; Tougerti, A.; Fonda, E.; Girardon, J.-S.; Paul, J.-F.; Mamede, A.-S.; Berrier, E. Mn- or Cu- Substituted $LaFeO_3$-Based Three-Way Catalysts: Highlighting Different Catalytically Operating Modes of $La_{0.67}Fe_{0.8}M_{0.2}O_3$ (M=Cu, Mn). *Appl. Catal., B* **2021**, *296*, No. 120330.

(19) Wu, J.; Dacquin, J.-P.; Djelal, N.; Cordier, C.; Dujardin, C.; Granger, P. Calcium and Copper Substitution in Stoichiometric and La-Deficient $LaFeO_3$ Compositions: A Starting Point in Next Generation of Three-Way-Catalysts for Gasoline Engines. *Appl. Catal., B* **2021**, *282*, No. 119621.

(20) Chatterjee, D.; Deutschmann, O.; Warnatz, J. Detailed Surface Reaction Mechanism in a Three-Way Catalyst. *Faraday Discuss.* **2001**, *119*, 371−384.

(21) Shelef, M.; Graham, G. W. Why Rhodium in Automotive Three-Way Catalysts? *Catal. Rev.* **1994**, *36*, 433−457.
(22) Brown, W. A.; King, D. A. NO Chemisorption and Reactions on Metal Surfaces: A New Perspective. *J. Phys. Chem. B* **2000**, *104*, 2578−2595.
(23) Takagi, N.; Ishimura, K.; Fukuda, R.; Ehara, M.; Sakaki, S. Reaction Behavior of the NO Molecule on the Surface of an M_n Particle (M = Ru, Rh, Pd, and Ag; n = 13 and 55): Theoretical Study of Its Dependence on Transition-Metal Element. *J. Phys. Chem. A* **2019**, *123*, 7021−7033.
(24) Kapteijn, F.; Stegenga, S.; Dekker, N. J. J.; Bijsterbosch, J. W.; Moulijn, J. A. Alternatives to Noble Metal Catalysts for Automotive Exhaust Purification. *Catal. Today* **1993**, *16*, 273−287.
(25) Severino, F.; Brito, J. L.; Laine, J.; Fierro, J. L. G.; Agudo, A. L. Nature of Copper Active Sites in the Carbon Monoxide Oxidation on $CuAl_2O_4$ and $CuCr_2O_4$ Spinel Type Catalysts. *J. Catal.* **1998**, *177*, 82−95.
(26) Stefanov, P.; Avramova, I.; Stoichev, D.; Radic, N.; Grbic, B.; Marinova, T. Characterization and Catalytic Activity of Cu−Co Spinel Thin Films Catalysts. *Appl. Surf. Sci.* **2005**, *245*, 65−72.
(27) Zhou, C.; Zhang, Y.; Hu, L.; Yin, H. Guo Wang, W., Synthesis, Characterization, and Catalytic Activity of Mn-Doped Perovskite Oxides for Three-Way Catalysis. *Chem. Eng. Technol.* **2015**, *38*, 291−296.
(28) Yoshida, H.; Hirakawa, T.; Oyama, H.; Nakashima, R.; Hinokuma, S.; Machida, M. Effect of Thermal Aging on Local Structure and Three-Way Catalysis of Cu/Al_2O_3. *J. Phys. Chem. C* **2019**, *123*, 10469−10476.
(29) Simmance, K.; Thompsett, D.; Wang, W.; Thiebaut, B. Evaluation of Perovskite Catalysts Prepared by Flame Spray Pyrolysis for Three-Way Catalyst Activity under Simulated Gasoline Exhaust Feeds. *Catal. Today* **2019**, *320*, 40−50.
(30) Yoshida, H.; Yamashita, N.; Ijichi, S.; Okabe, Y.; Misumi, S.; Hinokuma, S.; Machida, M.; Thermally, A. Stable Cr−Cu Nanostructure Embedded in the CeO_2 Surface as a Substitute for Platinum-Group Metal Catalysts. *ACS Catal.* **2015**, *5*, 6738−6747.
(31) Koizumi, K.; Yoshida, H.; Boero, M.; Tamai, K.; Hosokawa, S.; Tanaka, T.; Nobusada, K.; Machida, M. A Detailed Insight into the Catalytic Reduction of NO Operated by Cr−Cu Nanostructures Embedded in a CeO_2 Surface. *Phys. Chem. Chem. Phys.* **2018**, *20*, 25592−25601.
(32) Yoshida, H.; Okabe, Y.; Misumi, S.; Oyama, H.; Tokusada, K.; Hinokuma, S.; Machida, M. Structures and Catalytic Properties of Cr−Cu Embedded CeO_2 Surfaces with Different Cr/Cu Ratios. *J. Phys. Chem. A* **2016**, *120*, 26852−26863.
(33) Takagi, N.; Ishimura, K.; Miura, H.; Shishido, T.; Fukuda, R.; Ehara, M.; Sakaki, S. Catalysis of Cu Cluster for NO Reduction by CO: Theoretical Insight into the Reaction Mechanism. *ACS Omega* **2019**, *4*, 2596−2609.
(34) Takagi, N.; Ehara, M.; Sakaki, S. Theoretical Study of NO Dissociative Adsorption onto 3*d* Metal Particles M_{55} (M = Fe, Co, Ni, and Cu): Relation between the Reactivity and Position of the Metal Element in the Periodic Table. *ACS Omega* **2021**, *6*, 4888−4898.
(35) Kang, C. Y.; Taniguchi, M.; Uenishi, M.; Tanaka, H. Synthesis and Properties of Ni−Cu Alloy Supported on Mg−Al Mixed Oxide Catalyst for Automotive Exhaust. *Chem. Lett.* **2012**, *41*, 822−824.
(36) Asakura, H.; Onuki, T.; Hosokawa, S.; Teramura, K.; Tanaka, T. Self-Regeneration Process of Ni−Cu Alloy Catalysts During a Three-Way Catalytic Reaction—an Operando Study. *ACS Appl. Mater. Interfaces* **2020**, *12*, 55994−56003.
(37) Hirakawa, T.; Shimokawa, Y.; Tokuzumi, W.; Sato, T.; Tsushida, M.; Yoshida, H.; Ohyama, J.; Machida, M. Multicomponent 3*d* Transition-Metal Nanoparticles as Catalysts Free of Pd, Pt, or Rh for Automotive Three-Way Catalytic Converters. *ACS Appl. Nano Mater.* **2020**, *3*, 9097−9107.
(38) Hirakawa, T.; Shimokawa, Y.; Miyahara, Y.; Tsushida, M.; Yoshida, H.; Ohyama, J.; Machida, M. Activity−Composition Relationships of Fe−Ni−Cu Ternary Nanoparticles Supported on Al_2O_3 as Three-Way Catalysts for NO Reduction. *ACS Appl. Nano Mater.* **2021**, *4*, 10613−10622.
(39) Papanikolaou, K. G.; Stamatakis, M. The Catalytic Decomposition of Nitrous Oxide and the NO + CO Reaction over Ni/Cu Dilute and Single Atom Alloy Surfaces: First-Principles Microkinetic Modelling. *Catal. Sci. Technol.* **2021**, *11*, 3681−3696.
(40) Ebel, M. F. X-Ray Measurements on Spinodal Decomposition in Cu−Ni Alloys. *Phys. Status Solidi A* **1971**, *5*, 91−94.
(41) Hargreaves, M. E. Modulated Structures in Some Copper-Nickel-Iron Alloys. *Acta Crystallogr.* **1951**, *4*, 301−309.
(42) Bye, G. C.; Simpkin, G. T. Influence of Cr and Fe on Formation of α-Al_2O_3 from γ-Al_2O_3. *J. Am. Ceram. Soc.* **1974**, *57*, 367−371.
(43) Bondioli, F.; Ferrari, A. M.; Leonelli, C.; Manfredini, T.; Linati, L.; Mustarelli, P. Reaction Mechanism in Alumina/Chromia (Al_2O_3−Cr_2O_3) Solid Solutions Obtained by Coprecipitation. *J. Am. Ceram. Soc.* **2004**, *83*, 2036−2040.
(44) Ozawa, M.; Kato, O.; Suzuki, S. The Effect of a Cr_2O_3-Addition on the Phase Transformation and Catalytic Properties of γ-Al_2O_3 in Treatment of Lean-Burn Exhausts. *J. Mater. Sci.* **1998**, *33*, 737−741.
(45) Hirakawa, T.; Tokuzumi, W.; Shimokawa, Y.; Sato, T.; Yoshida, H.; Ohyama, J.; Machida, M. Comparative Study of Structure-Catalytic Activity Relationship for Ni−Cr−Al−O and Cu−Ni−Cr−Al−O Spinel Oxide Solid Solutions. *J. Ceram. Soc. Jpn.* **2020**, *128*, 906−911.
(46) Brodén, G.; Rhodin, T. N.; Brucker, C.; Benbow, R.; Hurych, Z. Synchrotron Radiation Study of Chemisorptive Bonding of CO on Transition Metals — Polarization Effect on Ir(100). *Surf. Sci.* **1976**, *59*, 593−611.
(47) Root, T. W.; Schmidt, L. D.; Fisher, G. B. Adsorption and Reaction of Nitric Oxide and Oxygen on Rh(111). *Surf. Sci.* **1983**, *134*, 30−45.
(48) Garin, F. Mechanism of NO_x Decomposition. *Appl. Catal., A* **2001**, *222*, 183−219.
(49) Ravel, B.; Newville, M. Athena, Artemis, Hephaestus: Data Analysis for X-Ray Absorption Spectroscopy Using IFEFFIT. *J. Synchrotron Radiat.* **2005**, *12*, 537−541.

https://doi.org/10.1021/acsomega.2c05043
ACS Omega 2022, 7, 44869−44877